Tang et al. Nanoscale Research Letters (2015) 10:260
DOI 10.1186/s11671-015-0960-x

Nanoscale Research Letters
a SpringerOpen Journal

NANO EXPRESS Open Access

Synthesis of Mn_3O_4-Based Aerogels and Their Lithium-Storage Abilities

Huang Tang[1,2*], Yongxing Sui[1], Xiaoqin Zhu[1] and Zhihao Bao[2*]

Abstract

Mn_3O_4 aerogels and their graphene nanosheet (GN) composite aerogels were synthesized by a simple supercritical-ethanol process. In the process, supercritical ethanol acted as a reductant to reduce graphene oxide and MnO_2 gels simultaneously. The synthesized aerogels consisted of 10–20 nm Mn_3O_4 nanocrystallites, with BET-specific surface areas around 60 m^2/g. The performance of the aerogels as anode materials for lithium-ion batteries was also evaluated in this study. The results showed that Mn_3O_4 aerogels as anode materials exhibited a reversible capacity of 498.7 mAh/g after 60 charge/discharge cycles while the reversible capacity for Mn_3O_4/GN composite aerogels could further increase to 665 mAh/g. The mechanisms for the enhanced capacity retention could be attributed to their porous structures and improved electronic contact with GN addition. The process should also offer an effective and facile method to fabricate many other porous metal oxide/GN nanocomposites for low-cost, high-capacity, environmentally benign material for lithium-ion batteries.

Keywords: Mn_3O_4 aerogel; Graphene nanosheet; Lithium-ion batteries

Background

Nanostructured materials such as nanowires, nanotubes, nanosheets, and porous nanomaterials have attracted great interest in the recent years because of the novel properties from their reduced dimensionality. They are becoming increasingly important for electrochemical energy-storage applications, especially for lithium-ion batteries [1–5]. The advantages of using nanostructured materials as electrodes for lithium-ion batteries include short path lengths for electron and Li-ion diffusion for high power, and accommodation of the strain due to Li intercalation/extraction for good cycle life, and so on [6–8]. Aerogels are well-known nanostructured materials with very high surface areas. They have a three-dimensional network of nanosized particles surrounded by macro-, meso-, and micropores. The diffusion distances for lithium ions and electrons in the nanosized aerogel particles are expected to be shorter compared with that of the solid electrode materials. Electrolytes can also easily infiltrate the entire aerogel particles. Porous structures may accommodate the strain induced by the volume expansion during the lithiation process. The above characteristics could enhance the performance (i.e., cyclability and rate capability) of corresponding materials such as the electrodes for lithium-ion batteries. For example, V_2O_5 aerogels were reported to have electroactive capacities greater than polycrystalline-solid V_2O_5 powders [9]. Thereafter, other aerogels, including MnO_2 and Li_xMnO_2 as cathode materials for lithium-ion batteries, have also been investigated [10–12]. However, to our knowledge, the successful synthesis of Mn_3O_4 aerogels has not been reported and their lithium-storage abilities have not been studied so far. Mn_3O_4 is an attractive anode material for lithium-ion batteries due to high abundance of Mn element in natural resource, low cost, and environmental benignity. Its theoretical capacity can reach as high as ~936 mAh/g. However, previous studies reported that Mn_3O_4 showed poor performance as anode materials for lithium batteries. At a current density of 40 mA/g, the pure solid Mn_3O_4 powder showed a capacity lower than 300 mAh/g, which further decreased to ~200 mAh/g after ten cycles. Even for Co-doping Mn_3O_4, the first discharge capacity of ~900 mAh/g could be reached; however, it also further decreased to ~400 mAh/g after ten cycles [13]. Mn_3O_4 nanoparticles even showed worse performance.

* Correspondence: tangh@126.com; zbao@tongji.edu.cn
[1]School of Mathematics and Physics, Jiangsu University of Technology, 1801 Zhongwu Road, Changzhou 213001, China
[2]Shanghai Key Laboratory of Special Artificial Microstructure Materials and Technology, School of Physics Science and Engineering, Tongji University, 1239 Siping Road, Shanghai 200092, China

After 10 cycles, only a capacity of ~115 mAh/g was retained. Only recently, have the capacity and rate capability of Mn_3O_4 been greatly improved by wiring up the Mn_3O_4 nanoparticles through a two-step solution-phase method [14].

In this paper, we have synthesized Mn_3O_4 aerogels and its graphene composite aerogels for the first time by a straightforward method, a supercritical-ethanol process. The results indicate that the supercritical-ethanol process can not only serve as a drying method to obtain the porous structure of aerogels but also reduce high-valence manganese oxide and graphene oxide (GO) simultaneously. The lithium-storage abilities of Mn_3O_4 aerogels were also investigated. The anode based on pure Mn_3O_4 aerogels exhibited an initial capacity of 1274.3 mAh/g. After 60 discharge/charge cycles, the capacity of 498.7 mAh/g was retained while the capacity increased to 665 mAh/g when graphene nanosheets (GNs) were incorporated into aerogel structure to improve their electronic contact.

Methods

Synthesis of GO

GO was prepared by a modified Hummers method [15, 16]. Briefly, 1 g-powdered flake graphite (500 mesh) and 0.75 g of $NaNO_3$ were placed in a flask. 75 mL of H_2SO_4 (98 wt %) was then added with mechanical stirring in an ice-water bath. After 10 min, 4.5 g of $KMnO_4$ was added gradually in the flask in 1 h. After the mixture was stirred vigorously for 5 days at room temperature, 3 mL of H_2O_2 (30 wt % aqueous solution) was added, and the mixture was stirred for 2 h at room temperature. The mixture was washed thoroughly with a mixed aqueous solution of 3 wt % H_2SO_4/0.5 wt % H_2O_2 to remove the excess manganate and the sulfate. Then, the solution was subjected to dialysis for 3–4 days to completely remove residual metal ions and acids. A typical AFM of GO is shown in Additional file 1: Figure S1.

Synthesis of Mn_3O_4-Based Aerogels

MnO_2 wet gels were prepared by the previously reported method [17]. Briefly, 0.948 g of $KMnO_4$ was dissolved in 12.5-ml de-ion water. 0.232 fumaric acid was then added into the vigorously stirred $KMnO_4$ solution. The resulting brown sol was then poured into polypropylene molds for gelation and aging for 24 h. The gel then was rinsed in 1-M sulfuric acid, followed by multiple rinses with water to remove impurity. MnO_2/GO composite was prepared by adding GO into MnO_2 sol first. The rest of the gelation and aging procedures were the same. Wet gels were then rinsed with ethanol for several times. The rinsed MnO_2 gels and its graphene nanosheet (GN) hybrid were subjected to a supercritical-ethanol process at 260 °C at 10 MPa for 6 h to form Mn_3O_4 aerogels and Mn_3O_4/GN composite aerogels.

Characterization

X-ray diffraction (XRD) patterns were obtained by an X-ray diffractometer (Rigaku D/Max-RB) with high intensity Cu Kα radiation (λ = 1.5418 Å, 40 kV, 100 mA).The morphology of samples was observed by a scanning electron microscopy (SEM, JSM6700F). Transmission electron microscopy (TEM) was conducted with a JEOL JEM-2010 electron microscope operating at 200 keV. The GN content in the Mn_3O_4/GN composite was determined by a thermogravimeter (TG, SDT Q600), and the measurements were carried out in air over a temperature range of 30–500 °C with a ramp rate of 10 °C /min. X-ray photoelectron spectroscopy (XPS) experiments were carried out on a RBD-upgraded PHI-5000C ESCA system (Perkin Elmer) with Al Kα radiation (1486.6 eV). XPS Peak Version 4.1 software was used to perform curve fitting. The N_2 absorption-desorption analysis was conducted on an Autosorb-1 instrument. The distribution of pore size was calculated from the desorption data using the Barret-Joyner-Halenda (BJH) method.

Electrochemical Measurement

The powder of Mn_3O_4 aerogels and Mn_3O_4/GN composite aerogels as active materials, Super P carbon black and polyvinyldifluoride (weight ratio 80:10:10), were mixed in N-Methylpyrrolidone (NMP) solvent to produce an electrode slurry. The slurry was coated onto a copper foil using the doctor-blading method and then dried to form the working electrode. The electrochemical tests were performed using two-electrode coin-type cells with lithium as both the counter and reference electrode. 1 M of $LiPF_6$ in a 1:1:1 (volume ratio) mixture of ethylene carbonate and diethyl carbonate and dimethyl carbonate was used as the electrolyte. Cell assembling was carried out in an argon-filled glove box. Galvanostatic charge-discharge cycling was conducted using a battery tester (Land, CT2100A) with a voltage window of 3–0.01 V at the current density of 50 mA/g.

Results and Discussion

Synthesis and Characterization of Mn_3O_4 and Mn_3O_4/GN Composite Aerogels

The process for preparing Mn_3O_4 and Mn_3O_4/GN aerogels is illustrated schematically in Fig. 1. MnO_2 gels were prepared by adding fumaric acid to a stirred $KMnO_4$ solution, following the reaction below [18, 19]:

$$\begin{aligned} 3HOOCHC = {} & CHCOOH + 10MnO_4^- \\ & + 10H_3O^+ \rightarrow 10MnO_2 + 18H_2O \\ & + 6CO_2\uparrow + 3H_2C_2O_4 \end{aligned}$$

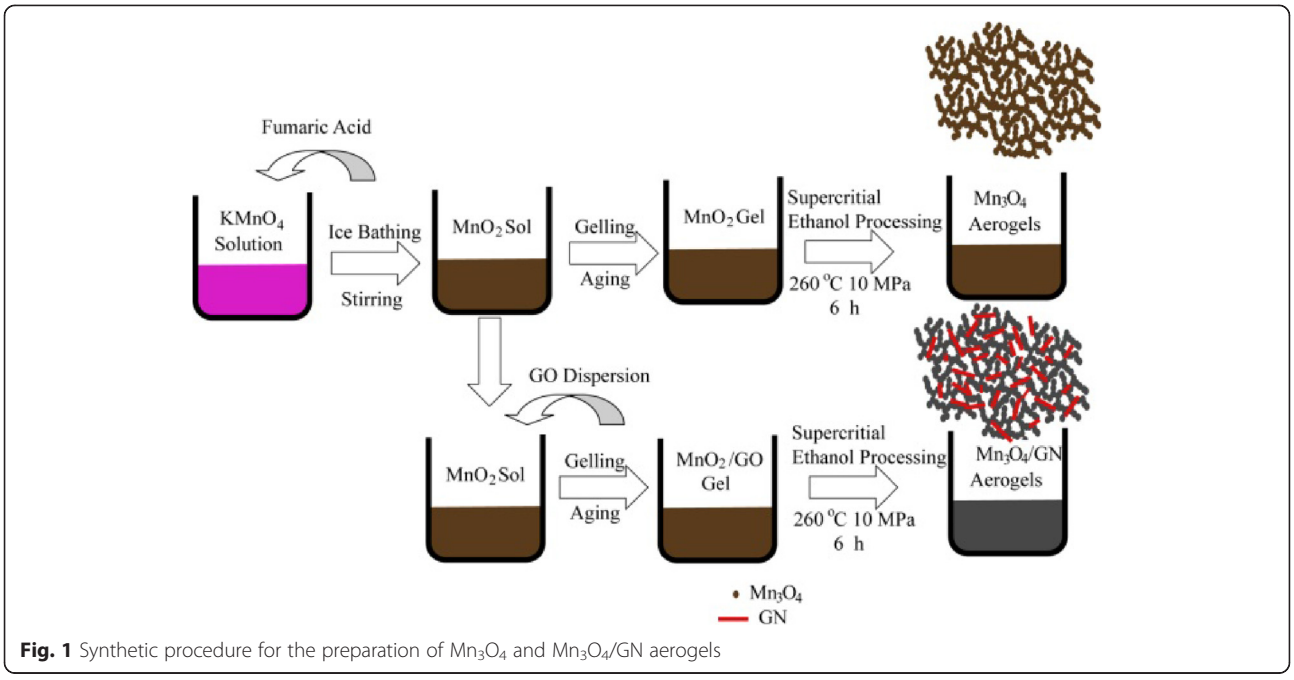

Fig. 1 Synthetic procedure for the preparation of Mn_3O_4 and Mn_3O_4/GN aerogels

as synthesized monoliths of Mn_3O_4 gels and Mn_3O_4/GN composite gels after the supercritical-ethanol process are brown and gray, respectively (Additional file 1: Figure S2). Figure 2a shows the XRD pattern of MnO_2 dried gel sample. The broad-peak profile indicates its amorphous nature. Broad peaks at $2\theta = 36.6°$, 37.5° and 65.8° can be indexed to α-MnO_2 (JCPDS No. 44–0141). After the supercritical-ethanol process (260 °C, 10 MPa), plenty of sharp peaks appear (Fig. 2b and c) and fit very well with the XRD pattern of Mn_3O_4 (JCPDS No. 24–0734), indicating formation of Hausmannite-type Mn_3O_4. No peaks of any other phases or impurities are observed, demonstrating that high-purity Mn_3O_4 can be obtained using the above method. According to Scherrier analysis, the size of Mn_3O_4 is estimated to be ~10 nm. The above results indicate that MnO_2 was reduced into Mn_3O_4. The

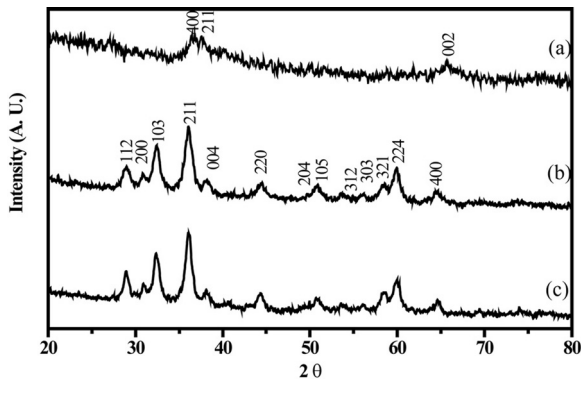

Fig. 2 X-ray diffraction patterns of MnO_2 dried gel **a**, Mn_3O_4 aerogels **b**, and Mn_3O_4/GN composite aerogels **c**

following chemical reaction was suggested to happen in the supercritical-ethanol process,

$$3MnO_2(s) + 2C_2H_5OH(l) \rightarrow Mn_3O_4(s) + 2CH_3COH(1) + 2H_2O(l)$$

Supercritical ethanol acted as the reducing agent to reduce MnO_2 into Mn_3O_4 during the process [20, 21]. Meanwhile, high pressure and high temperature facilitated the crystallization of Mn_3O_4.

At the same time, alcohols were reported as effective reductants to reduce GO into highly conductive GN [22, 23]. Thus, supercritical ethanol under high temperature and high pressure was expected to have improved reducibility to reduce GO pre-mixed in MnO_2 gels into GN. Here, XPS (Fig. 3) was used to analyze GO powder and GO in composite after the supercritical-ethanol process. Curve fitting of the spectra was performed using Gaussian-Lorentzian peak shape after a Shirley background correction. For GO, three peaks located at 284.6, 286.8, and 288.0 eV could be assigned to the C-C/C = C, C-O, and C = O species, respectively [24, 25]. The peak at 286.8 eV after supercritical-ethanol treatment almost disappeared, indicating that the C-O species were removed by the supercritical-ethanol process. Hydrogenating capacity of ethanol under the supercritical condition was responsible for the partial elimination of oxygen-containing functional groups on GO. The GN content in the Mn_3O_4/GN nanocomposite was quantitatively determined to be 7.3 wt % by thermogravimetric analysis (Additional file 1: Figure S3). Figure 4 shows SEM images of the Mn_3O_4 aerogels and Mn_3O_4/GN composite aerogels. Samples

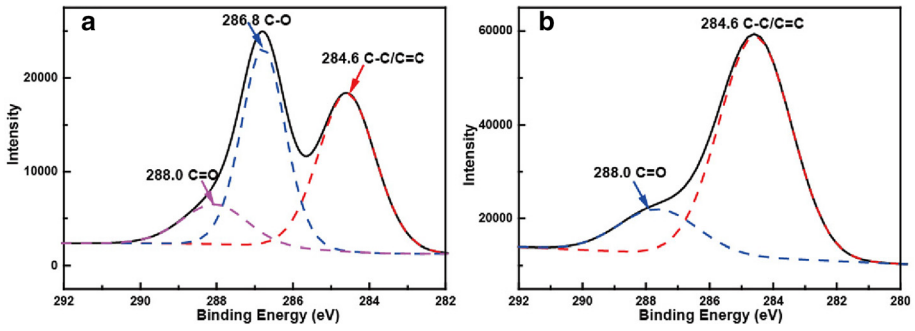

Fig. 3 XPS of graphene oxide **a** before and **b** after the supercritical-ethanol process

exhibited porous structures composed of 10–20 nm Mn_3O_4 nanoparticles. In Mn_3O_4/GN composite aerogels, the micron-sized reduced GO sheets randomly distributed, and a lot of Mn_3O_4 nanoparticles were attached on their surface. Due to its good solubility in the water solution, GO could be dispersed in the gels very well. Such GO was frozen in the gel structure and kept with good dispersion during the subsequent reduction in the supercritical-ethanol process. The process somewhat avoided the agglomeration problem, which usually accompanied the reduction of GO into GN in the solution.

The bright field TEM image (Fig. 5) of the resulting Mn_3O_4/GN nanocomposite products confirms that the 10–20 nm Mn_3O_4 nanoparticles decorated on the surface of GN. A selected area electron diffraction (SAED) pattern of the final products is shown in the insert of Fig. 5. All the concentric diffraction rings are related to the phase of Mn_3O_4, consistent with the relevant XRD analyses. Surface area, pore size, and pore volume are important characteristics for aerogel materials. The data related with Mn_3O_4 aerogels and Mn_3O_4/GN aerogels are summarized in Table 1. Nitrogen adsorption/desorption isotherms (Additional file 1: Figure S4) of the Mn_3O_4 aerogels and Mn_3O_4/GN composite aerogels are type IV isotherms with H1 hysteresis loops, which are characteristic of an interconnected mesoporous system with cylindrical pores. BET-specific surface areas are 69 and 67 m^2/g, respectively. The BET-specific areas are not as high as the reported value (~200 m^2/g) of MnO_2 aerogels [17], which might be due to crystallization and

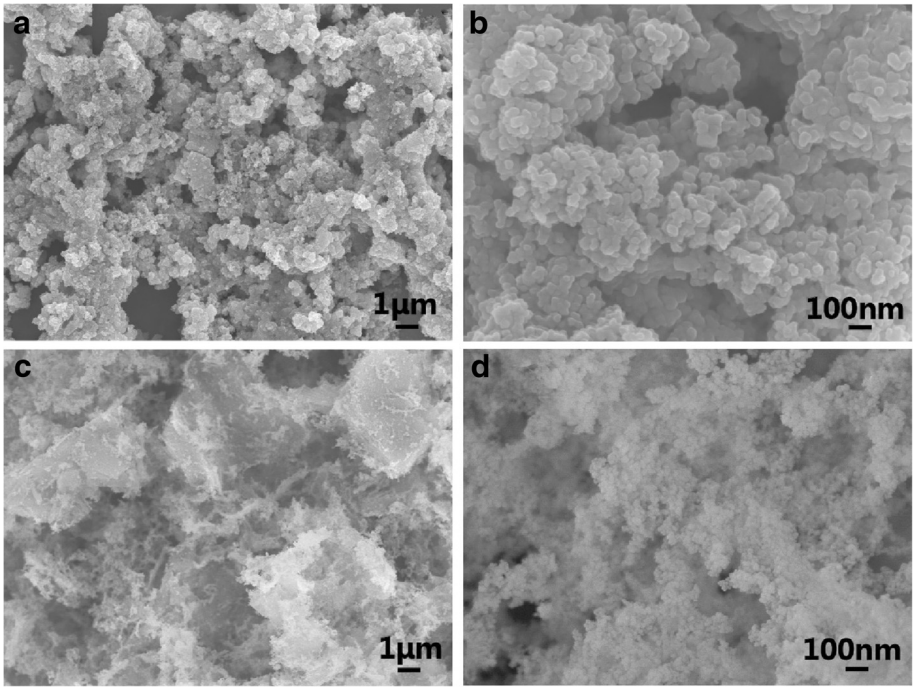

Fig. 4 SEM images of Mn_3O_4 aerogel particles and Mn_3O_4/GN composite aerogel particles: **a** low magnification image of the Mn_3O_4 aerogel particles; **b** high magnification of **a**; **c** low magnification image of the Mn_3O_4/GN composite aerogel particles; **d** high magnification of **c**

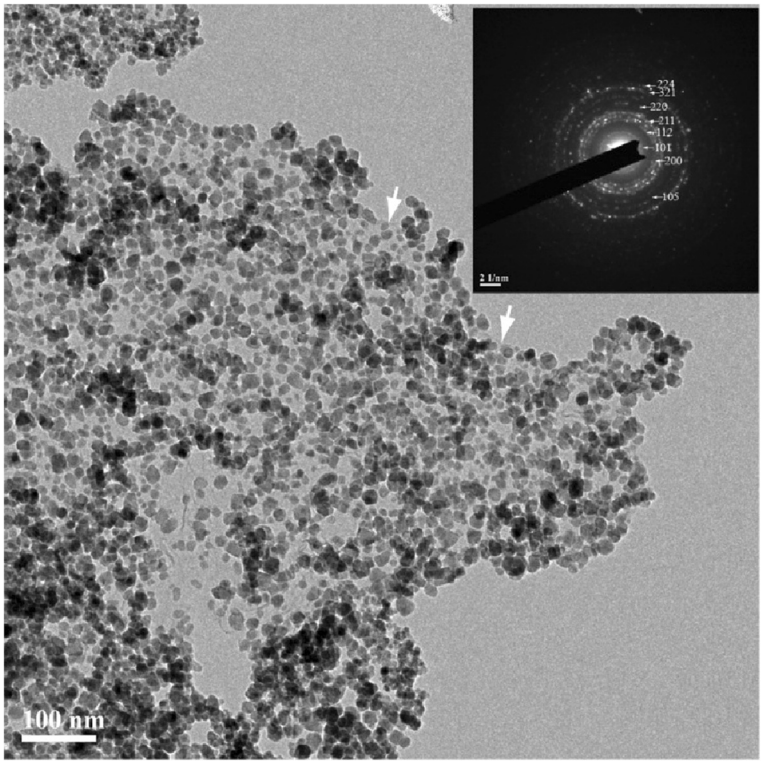

Fig. 5 Typical TEM image of Mn_3O_4/GN composite aerogels and their SAED pattern (*inset*). *White arrows* indicate the edges of GN

coarsening of Mn_3O_4 in the supercritical-ethanol process at relative high temperature and pressure.

Electrochemical Properties of Anodes Based on Mn_3O_4 Aerogels and Mn_3O_4/GN Composite Aerogels

To evaluate the electrochemical performance of Mn_3O_4-based aerogels, the samples were used as the anodes for Li-ion battery. Figure 6a,b show the charge and discharge curves for anodes based on Mn_3O_4 and Mn_3O_4/GN aerogels, respectively. In the first discharge curve, a sloping plateau in the range of ~1.5– 0.3 V is observed. It might be due to the formation of solid-electrolyte interface (SEI) film on the active materials. The well-defined voltage plateau around 0.35 V reflected the reduction reaction of Mn_3O_4 as follows: $Mn_3O_4 + 8Li^+ + 8e^- \rightarrow 3Mn(0) + 4Li_2O$ [26]. The charge curve shows a plateau at ~1.2 V due to the reverse reaction [14]. Figure 6c compares the cycle performance of Mn_3O_4 electrode and Mn_3O_4/GN electrode at a current of 50 mA/g. The Mn_3O_4 electrode shows an initial discharge capacity of 1274.3 mAh/g with an initial Coulombic efficiency of 51.7 %. With GN addition, the initial discharge capacity for Mn_3O_4/GN was measured to be 1134.2 mAh/g with an initial Coulombic efficiency of 58.7 %. The capacity loss results from the formation of SEI film, some other irreversible side-reactions, and the disengagement of the Mn_3O_4 particles from the electrodes. After 60 cycles, the Mn_3O_4/GN composite electrode retained a discharge capacity of 665 mAh/g with a Coulombic efficiency of 97.7 %, compared with the Mn_3O_4 electrode with a discharge capacity of 498.7 mAh/g with a Coulombic efficiency of 97.2 %. The specific capacities of Mn_3O_4 and Mn_3O_4/GN are both much higher than the reported values of the anode based on Mn_3O_4 nanoparticles, 115 mAh/g after ten cycles [14]. The improved electrochemical performance of Mn_3O_4 aerogels could be attributed to the structure of aerogels. The high porosity from mesopores of aerogel structures facilitates the transportation of lithium ions in the aerogel particle, and the large surface area of aerogel enhances the utilization of active materials [27]. Further improvement of electrochemical properties of Mn_3O_4/GN can be attributed to the wiring effect of

Table 1 Summary of N_2 adsorption/desorption data for Mn_3O_4 aerogels and Mn_3O_4/GN composite aerogels

Sample	Specific surface area	Pore volume	Average pore diameter
	(m^2/g)	(cm^3/g)	(nm)
Mn_3O_4 aerogels	69	0.25	14.5
Mn_3O_4/GN aerogels	67	0.27	16.1

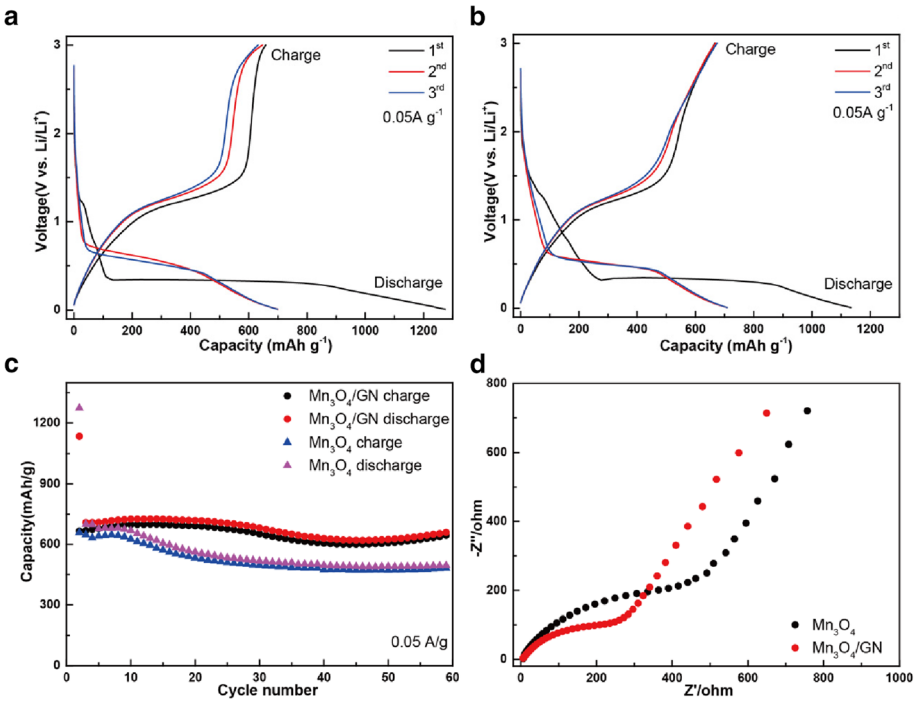

Fig. 6 Galvanostatic charge-discharge voltage profiles of anodes based on Mn_3O_4 aerogels **a** and Mn_3O_4/GN composite aerogels **b**, cycle performance of Mn_3O_4 aerogels and Mn_3O_4/GN composite aerogels **c**, and Nyquist plots of the Mn_3O_4 and Mn_3O_4/GN electrodes **d**

GN, that is, that the large-sized GNs can build an excellent conductive network which facilitates the electron transfer in the structure of aerogels. This was supported by electrochemical impedance spectroscopy (EIS) measurements performed after the fifth cycle. The Nyquist plots of the Mn_3O_4 and Mn_3O_4/GN electrodes are presented in Fig. 6d. Both Nyquist plots consist of one semicircle at medium-frequency region, which could be related to charge-transfer resistance [28]. The diameter of the semicircle of Mn_3O_4/GN electrode is smaller than that of pure a Mn_3O_4 electrode, indicating the enhanced electron conductivity of the Mn_3O_4/GN [29].

Conclusions

Mn_3O_4 aerogels and its GN composite aerogels were synthesized by the simple supercritical-ethanol process on MnO_2 and MnO_2/GO gels, respectively. Supercritical ethanol served as both drying and reducing agents of MnO_2 and GO in the process. The samples were characterized by X-ray, SEM, XPS, and TEM. The electrochemical measurements demonstrated that Mn_3O_4 aerogels possessed better capacity retention compared with Mn_3O_4 nanoparticles. The enhanced performance of the synthesized Mn_3O_4 was ascribed to its porous aerogel structure. With GN addition to Mn_3O_4 aerogels, their electrochemical property was improved further. The higher capacity retention was attributed to the fact that GNs enhanced the electron transfer and reduced the resistance within Mn_3O_4. The process should also offer an effective and convenient technique to fabricate many other metal oxide/graphene porous nanocomposites for low-cost, high-capacity, environmentally benign material for lithium-ion batteries.

Additional file

Additional file 1: The AFM image of GO, the photo of Mn_3O_4 aerogel monoliths, and the thermogravimetric analyses and Nitrogen adsorption/desorption isotherms of Mn_3O_4 aerogel. Figure S1. AFM image of GO, **Figure S2.** Photos of monoliths of Mn_3O_4-based aerogels, **Figure S3.** Thermogravimetric analyses of Mn_3O_4-based aerogels, **Figure S4.** N2 isotherms and pore size distributions of Mn_3O_4-based aerogels.

Competing interests

The authors declare that they have no competing interests.

Authors' contributions

HT and ZB designed the experiment. HT, YS, and XZ performed the experiments. HT and ZB analyzed the data and wrote the manuscript. All authors read and approved the final manuscript.

Acknowledgements

This work was supported by the Scientific Research Foundation for Returned Scholars, the Ministry of Education of China, Key Basic Research Projects of Science and Technology Commission of Shanghai (no. 11JC1412900), and the National Science Foundation of China program (no. 21271140, 51472182). Thank Dr. Suyang Yu for help on the experiment.

Received: 17 March 2015 Accepted: 28 May 2015
Published online: 10 June 2015

References

1. Chan CK, Peng HL, Liu G, McIlwrath K, Zhang XF, Huggins RA, et al. High-performance lithium battery anodes using silicon nanowires. Nat Nanotechnol. 2008;3:31–5.
2. Honma I, Yoo E, Kim J, Hosono E, Zhou H, Kudo T. Large reversible li storage of graphene nanosheet families for use in rechargeable lithium ion batteries. Nano Lett. 2008;8:2277–82.
3. Ajayan PM, Reddy ALM, Shaijumon MM, Gowda SR. Coaxial MnO_2/carbon nanotube array electrodes for high-performance lithium batteries. Nano Lett. 2009;9:1002–6.
4. Ji XL, Lee KT, Nazar LF. A highly ordered nanostructured carbon-sulphur cathode for lithium-sulphur batteries. Nat Mater. 2009;8:500–6.
5. Li JH, Li YM, Lv XJ, Lu J. Preparation of SnO_2-nanocrystal/graphene-nanosheets composites and their lithium storage ability. J Phys Chem C. 2010;114:21770–4.
6. Chen J, Cheng FY. Combination of lightweight elements and nanostructured materials for batteries. Acc Chem Res. 2009;42:713–23.
7. Arico AS, Bruce P, Scrosati B, Tarascon JM, Van Schalkwijk W. Nanostructured materials for advanced energy conversion and storage devices. Nat Mater. 2005;4:366–77.
8. Bruce PG, Scrosati B, Tarascon JM. Nanomaterials for rechargeable lithium batteries. Angewandte Chemie-International Edition. 2008;47:2930–46.
9. Dong W, Rolison DR, Dunn B. Electrochemical properties of high surface area vanadium oxide aerogels. Electrochem Solid State Lett. 2000;3:457–9.
10. Owens BB, Passerini S, Smyrl WH. Lithium ion insertion in porous metal oxides. Electrochim Acta. 1999;45:215–24.
11. Kim J, Manthiram A. Nanocomposite manganese oxides for rechargeable lithium batteries. Electrochem Solid State Lett. 1998;1:207–9.
12. Dong W, Sakamoto J, Dunn B. Electrochemical properties of vanadium oxide aerogels and aerogel nanocomposites. J Sol–gel Sci Technol. 2003;26:641–4.
13. Pasero D, Reeves N, West AR. Co-doped Mn_3O_4: a possible anode material for lithium batteries. J Power Sources. 2005;141:156–8.
14. Wang H, Cui L-F, Yang Y, Sanchez Casalongue H, Robinson JT, Liang Y, et al. Mn_3O_4-graphene hybrid as a high-capacity anode material for lithium ion batteries. J Am Chem Soc. 2010;132:13978–80.
15. Hontorialucas C, Lopezpeinado AJ, Lopezgonzalez JDD, Rojascervantes ML, Martinaranda RM. Study of oxygen-containing groups in a series of graphite oxides—physical and chemical characterization. Carbon. 1995;33:1585–92.
16. Paek SM, Yoo E, Honma I. Enhanced cyclic performance and lithium storage capacity of SnO_2/graphene nanoporous electrodes with three-dimensionally delaminated flexible structure. Nano Lett. 2009;9:72–5.
17. Rolison D, Long J W, Lyons K S, Rolison D R. Amorphous lithium-manganese oxide anode. WO200230825-A; WO200230825-A1; AU200196760-A; US2121-H, 2002.
18. Bach S, Henry M, Baffier N, Livage J. Sol-gel synthesis of manganese oxides. J Solid State Chem. 1990;88:325–33.
19. Sugantha M, Ramakrishnan PA, Hermann AM, Warmsingh CP, Ginley DS. Nanostructured MnO_2 for li batteries. Int J Hydrog Energy. 2003;28:597–600.
20. Buslaeva EY, Kravchuk KG, Kargin YF, Gubin SP. Reactions of MnO2, Mn2O3, alpha-Bi2O3 and Bi12Ti1-xMnxO20 with supercritical isopropanol. Inorg Mater. 2002;38:582–5.
21. Zhang WX, Wang C, Zhang XM, Xie Y, Qian YT. Low temperature synthesis of nanocrystalline Mn_3O_4 by a solvothermal method. Solid State Ion. 1999;117:331–5.
22. Bielawski CW, Dreyer DR, Murali S, Zhu YW, Ruoff RS. Reduction of graphite oxide using alcohols. J Mater Chem. 2011;21:3443–7.
23. Li LJ, Su CY, Xu YP, Zhang WJ, Zhao JW, Liu AP, et al. Highly efficient restoration of graphitic structure in graphene oxide using alcohol vapors. ACS Nano. 2010;4:5285–92.
24. Paredes JI, Villar-Rodil S, Solis-Fernandez P, Martinez-Alonso A, Tascon JMD. Atomic force and scanning tunneling microscopy imaging of graphene nanosheets derived from graphite oxide. Langmuir. 2009;25:5957–68.
25. Ventrice CA, Yang D, Velamakanni A, Bozoklu G, Park S, Stoller M, et al. Chemical analysis of graphene oxide films after heat and chemical treatments by x-ray photoelectron and micro-raman spectroscopy. Carbon. 2009;47:145–52.
26. Ren WC, Wu ZS, Wen L, Gao LB, Zhao JP, Chen ZP, et al. Graphene anchored with Co_3O_4 nanoparticles as anode of lithium ion batteries with enhanced reversible capacity and cyclic performance. ACS Nano. 2010;4:3187–94.
27. Gao J, Lowe MA, Abruna HD. Spongelike nanosized Mn_3O_4 as a high-capacity anode material for rechargeable lithium batteries. Chem Mater. 2011;23:3223–7.
28. Rahman MM, Wang JZ, Idris NH, Chen ZX, Liu HK. Enhanced lithium storage in a VO_2(b)-multiwall carbon nanotube microsheet composite prepared via an in situ hydrothermal process. Electrochim Acta. 2010;56:693–9.
29. Tang H, Gao P, Xing A, Tian S, Bao Z. One-pot low-temperature synthesis of a $MnFe_2O_4$-graphene composite for lithium ion battery applications. RSC Advances. 2014;4:28421–5.